Carbohydrate Polymers 326 (2024) 121586

Contents lists available at ScienceDirect

Carbohydrate Polymers

journal homepage: www.elsevier.com/locate/carbpol

A bioinspired and sustainable route for the preparation of Ag-crosslinked alginate fibers decorated with silver nanoparticles

Pietro Tordi [a,b], Rita Gelli [a], Francesca Ridi [a], Massimo Bonini [a,*]

[a] Department of Chemistry "Ugo Schiff" and CSGI, University of Florence, via della Lastruccia 3, 50019 Sesto Fiorentino, Florence, Italy
[b] Institut de Science et d'Ingeniérie Supramoléculaires (ISIS) - Université de Strasbourg and CNRS, 8 Alleé Gaspard Monge, F-67000 Strasbourg, France

ARTICLE INFO

Keywords:
Alginate
Silver-NPs
Citric acid
Ascorbic acid
Fibers
Bioinspired

ABSTRACT

Functional materials obtained through green and sustainable routes are attracting particular attention due to the need to reduce the environmental impact of the chemical industry. In this work we propose a bioinspired approach for the preparation of alginate fibers containing silver nanoparticles (AgNPs), to be used for antimicrobial purposes. We demonstrate that filiform polymeric structures with length of a few meters can be easily obtained by extruding an alginate solution in an aqueous Ag^{+}-containing bath (*i.e.* wet spinning) and that treating the fibers with freshly-squeezed lemon juice leads to the formation of AgNPs homogeneously distributed within the polymeric network. Using mixtures of ascorbic and citric acid to mimic lemon juice composition we highlight the influence of the aforementioned molecules on the nanoparticles formation process as well as on the properties of the fibers. Varying the amount of citric and ascorbic acid used for the treatment allows to finely tune the thermal, morphological and water absorption properties of the fibers. This evidence, along with the possibility to easily monitor the preparation through FT-IR spectroscopy, endows the fibers with a high application potential in several fields such as wound healing, water/air purification and agriculture.

1. Introduction

Alginate is an anionic polysaccharide discovered by E.C.C. Stanford in 1881 (Stanford, 1881). It is commonly obtained through alkaline extraction from brown algae belonging to the *Phaeophyceae* class (Yoon et al., 2009), but its occurrence in some bacteria is also reported (Skjåk-Bræk et al., 1986). Alginate is considered safe by the *Food and Drug Administration* (FDA), which classifies it as a food additive. This characteristic, combined with its biodegradability and biocompatibility, makes alginate suitable to be used in the medical, cosmetic, agricultural and food sectors. The structure of this polymer consists of (1,4) linked β-D-Mannuronate (M) and α-L-Guluronate (G) residues and can be elucidated through both ^{1}H and ^{13}C NMR analyses (Grasdalen, 1983; Grasdalen et al., 1979, 1981; Salomonsen et al., 2009). The extraction source directly influences the M/G ratio (Aarstad et al., 2013; Huang & Larsen, 1962; Haug et al., 1967; Grasdalen et al., 1981) and the sequence of the residues. Homogeneous (GG or MM) and heterogeneous (GM or MG) blocks can coexist in the same polymeric chain (Grasdalen et al., 1981). The carboxylate moieties of the residues can strongly interact with cationic species to form complexes with various geometries: this phenomenon is commonly called crosslinking and is a simple approach to obtain hydrogels. It is interesting to note that the nature of the complex is strongly influenced by the nature of the ion in terms of charge and dimensions and by the sequence of the M and G residues. Alginate is reportedly able to crosslink with specific monovalent (Lengert et al., 2017), divalent (Haug & Smidsrød, 1965), trivalent (Singh et al., 2014; Zhou et al., 2014) and tetravalent cations (Elhoudi et al., 2022; Qing et al., 2022) to form hydrogel structures, whose properties depend on both the ion and the complex characteristics.

Among the ions able to crosslink with alginate, silver is particularly attractive for its antimicrobial properties both in nanoparticle (NP) and cationic form (Durán et al., 2016). The high specific surface allows the NPs to cap and disrupt bacterial membranes, releasing at the same time silver cations. The cytotoxicity of AgNPs, largely attributable to the generation of reactive oxygen species (ROS), increases as the NP dimension decreases (Durán et al., 2016). The chemical reduction of

Abbreviations: Alg, Alginate; Ag, Silver; NPs, Nanoparticles; CA, Citric acid; AA, Ascorbic acid; MW, Molecular weight; RH, Relative humidity; RT, Room temperature; TGA, Thermogravimetric analysis; FT-IR, Fourier transform-infrared; SR, Swelling ratio; FE-SEM, Field emission scanning electron microscopy; FIB, Fraction of ionic bonding; DSC, Differential scanning calorimetry; SD, Standard deviation.

* Corresponding author.
E-mail address: massimo.bonini@unifi.it (M. Bonini).

https://doi.org/10.1016/j.carbpol.2023.121586
Received 30 July 2023; Received in revised form 17 October 2023; Accepted 10 November 2023
Available online 13 November 2023

silver salts is the most common strategy to obtain AgNPs, although the toxic and polluting character of most of the chemicals commonly used is a remarkable drawback to this approach. In order to overcome this limitation, bioinspired strategies involving microorganisms (El-Naggar et al., 2017; Sivasankar et al., 2018) and plant extracts (Mane Gavade et al., 2015; Ravichandran et al., 2019) were developed in the last decades. In this context, AgNPs with predictable particle size were successfully synthesized using *Citrus lemon* extracts (Prathna et al., 2011). The reducing agents present in lemon juice which are responsible for the formation of AgNPs are reported to be citric acid (CA) and ascorbic acid (AA) (Ortega et al., 2021). However, there is no consensus on the role of the two components, some studies indicating the reducing role being mainly due to the CA (Prathna et al., 2011). Although alginate composite materials containing AgNPs were already reported in the literature (Ambrogi et al., 2020; Lin et al., 2013; Porter et al., 2021), alginate crosslinking with silver cations has been scarcely investigated so far. The high ionic radius of Ag^+ (1.15 Å) (Shannon, 1976) and the consequent soft character of this ion reduce both the number of binding sites and the interaction strength with the polymeric chains, hampering the preparation of complex-shaped hydrogel structures (*e.g.* fibers).

The aim of this paper is the design, preparation and characterization of alginate fibers crosslinked with silver ions and containing AgNPs. We want to demonstrate that a wet spinning approach can be used to easily produce filiform hydrogel structures with lengths up to some meters, due to the possibility of varying multiple preparation parameters. To obtain AgNPs formation on the alginate fibers, bioinspired solutions of CA and AA are used, mimicking the composition of the lemon juice (Prathna et al., 2011). Our work aims to unravel the effect of different CA/AA ratios on the features of both the fibers and the obtained Ag nanostructures, to prepare products attractive for the development of antimicrobial materials useful in wound healing, agriculture and water/air purification.

2. Materials and methods

2.1. Materials

Alginic acid sodium salt was purchased from Sigma Aldrich (Product number 180947. Mannuronate/Guluronate = 1.50 ± 0.04, determined through FT-IR spectroscopy (Gómez-Ordóñez & Rupérez, 2011; Sakugawa et al., 2004; Vetrano et al., 2022) (see Fig. S1 and Table S1 in the Supplementary Material). Molecular weight ≃ 132 kDa, determined through viscosimetric analysis (Masuelli & Illanes, 2014; Vetrano et al., 2022) (see Table S2 in the Supplementary Material). Silver nitrate ($AgNO_3$, Assay >99.8 %) was obtained from Carlo Erba. AA (Assay ≥99.0 %) was provided by Fluka, while CA monohydrate (min. 99.8 %) was purchased by J. T. Baker. Alginic acid from brown algae was provided by Sigma Aldrich (product number 1003449856). Controlled 95 % relative humidity (RH95) conditions were obtained using KNO_3 (Merck, Gehalt min. 99 %) supersaturated solutions in deionized water. Deionized water was used to prepare the sodium alginate, silver nitrate and CA-AA solutions. All reagents were used without any further purification.

2.2. Preparation of crosslinked alginate fibers containing silver nanostructures

2.2.1. Ag^+-crosslinked alginate fibers preparation

A 4 % (*w/v*) sodium alginate (MW Mannuronate/Guluronate unit = 193.12 $gmol^{-1}$) water solution was prepared by dissolving the polymer at room temperature under stirring for about 40 min. The solution was used to fill a 10 mL syringe and extruded through a needle (0.9 mm of internal diameter) in 50 mL of $AgNO_3$ 0.5 M. The extrusion process was carried out using a HYREL 3D Engine SR injection 3D printer equipped with an SDS-10 print head provided with an electric motor (model LDO-28STH51-0674 A). The extrusion flux was equal to 5.76 mL/min: 4.8 mL of polymeric solution were extruded for each batch, leading to a Ag-alginate fiber with a length of ~2.5 m. The instantaneously formed fiber was kept immersed in the silver nitrate solution for 1.5 h. The hydrogel was then washed with deionized water (5 mL/cm of fiber) for 1 h, to remove the excess of uptaken silver. Both the crosslinking and the washing steps were carried out in the dark to avoid any potential effect of light towards Ag^+ reduction. The samples' preparation is schematized in Fig. 1.

2.2.2. Ag^+ ions reduction

The washed Ag^+-crosslinked fibers were treated for 0.5 h in solutions containing different amounts of CA and AA (see Table 1), taking a cue from the lemon juice composition. For each sample, 30 cm of fiber was treated in 30 mL of solution. During the reduction, the solutions were periodically shaken to homogenize the treatment. The fibers were then washed for 1 h in deionized water (5 mL/cm of fiber). Both the reduction and the washing steps were carried out in the dark. Samples were either dried under the fume hood overnight or lyophilized. As a proof of concept, a portion of Ag-alginate fiber was reduced using fresh lemon juice, obtained by squeezing and filtering commercial lemons.

2.3. Characterization techniques

2.3.1. Evaluation of the color during the reduction

To monitor the color change during the reduction, 2 cm of Ag-alginate fibers were put in contact with 2 mL of the reducing solutions (see the composition in Table 1) in plastic cuvettes, and photos were taken at regular intervals for 30 min. A white-balance operation was carried out on the images using a graphic editor software, according to a white reference present in all photos. The color variation in time was quantified by converting the photos in 8-bit (*i.e.,* conversion in gray-scale), and applying an auto-contrast operation using the software *ImageJ*. The gray values of the fibers at half of their height were sampled, and plotted for each sample as a function of time.

2.3.2. Evaluation of the fibers diameter

The diameter of the fibers immediately after preparation and when dried was measured with a digital microscope from Park Systems. For each image, 10 measurements of the diameter were collected along the fiber, and the results are expressed as average ± standard deviation (SD). *ImageJ* software was used to analyze the data.

2.3.3. Swelling tests

To evaluate the swelling properties of the samples, 20 cm of dry fiber were weighted and then placed in 200 mL of deionized H_2O. Mass measurements were then acquired at regular intervals, extracting the samples from the fluid and removing the excess water by means of paper towel. The experiments were interrupted when a stable weight was attained for each sample. The swelling ratio (SR) was calculated according to Eq. (1):

$$SR = \frac{m_t - m_0}{m_0} \quad (1)$$

where m_t is the mass of the swollen sample at time t and m_0 is the initial (*i.e.,* dry) mass of the sample. For the determination of the SR at the equilibrium, measurements were performed in triplicate.

2.3.4. Field emission-scanning electron microscopy (FE-SEM)

Field emission-scanning electron microscopy (FE-SEM) analysis was conducted using a Zeiss ΣIGMA FE-SEM (Carl Zeiss Microscopy GmbH). The fibers, either lyophilized or air dried, were placed over aluminum stubs by means of conductive tape. The micrographs were acquired with an accelerating voltage of 2 kV, sample-detector distance 2–4 mm, aperture 10 μm and using the In-Lens detector. Energy dispersive X-ray spectroscopy (EDX) analysis was carried out with an X-act Silicon Drift

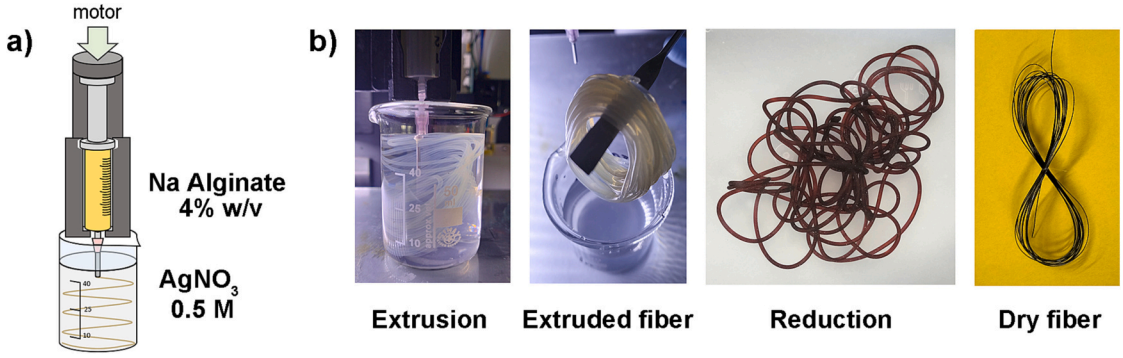

Fig. 1. a) Sketch of the extrusion process with the 3D printer. b) Photos of the different stages of fiber preparation.

Table 1
Nomenclature and composition of the solutions for the Ag-alginate fibers reduction. The pH of the AA solution is 3.73 ± 0.01, while that of all the CA-containing solutions is 1.99 ± 0.01 (experimental error of the pH-meter).

Sample	CA/AA (mol)	Citric acid (mg/mL)	Ascorbic acid (mg/mL)
AgAlg	–	–	–
AgAlg_AA	0	0	0.42
AgAlg_CA/AA = 5	5	48.18	8.83
AgAlg_CA/AA = 25	25	48.18	1.77
AgAlg_CA/AA = 50	50	48.18	0.88
AgAlg_CA/AA = 105	105	48.18	0.42
AgAlg_CA/AA = 150	150	48.18	0.29
AgAlg_CA/AA = ∞	∞	48.18	0

Detector (Oxford Instruments), using an accelerating voltage of 10 kV, a working distance of about 8 mm and an aperture of 60 μm. For each sample, three different sites were analyzed, and the average ± SD is reported.

2.3.5. X-ray diffraction (XRD)

XRD patterns were collected with a D8 Advance with DAVINCI design (Bruker), using as X-ray source the Cu Kα radiation (wavelength k = 1.542 Å) operating at 40 kV and 40 mA. The 2θ range was 30–80°, the step size 0.03° and the time/step 0.3 s. Before the analysis, the lyophilized fibers were cut into small pieces, grinded and flattened on a Si zero-background sample holder.

2.3.6. Fourier transform - infrared spectroscopy (FT-IR)

FT-IR spectra were collected using a Nexus 870 FT-IR spectrophotometer equipped with an ATR (Attenuated Total Reflectance) Golden Gate accessory. All the spectra were recorded at room temperature within the wavenumber range of 4000–650 cm^{-1} with a spectral resolution of 2 cm^{-1} and recording 128 scans for measurement.

2.3.7. Thermogravimetric analysis (TGA)

Thermogravimetric analysis was performed using Discovery SDT650 (TA Instruments). A heating ramp from room temperature (RT) to 1000 °C, with a rate of 10 °C/min, was applied to all the samples previously equilibrated at RH95. For the water content determination in the air dried samples, a heating ramp from RT to 200 °C (rate of 10 °C/min) was applied. Measurements were performed under N_2 flux (100 mL/min), using alumina pan. Data were analyzed with Trios v5.1.1.46572 software (TA Instruments). To determine the silver content of the fibers, a heating ramp from RT to 1000 °C, with a rate of 20 °C/min, was applied to all the samples under air flux (100 mL/min). Measurements were performed in duplicate. Data were analyzed with Trios v5.1.1.46572 software (TA Instruments).

2.3.8. Differential scanning calorimetry (DSC)

DSC analysis was carried out by means of Discovery DSC 2500 (TA Instruments). Tzero Aluminum Hermetic pan (TA Instruments) were used for all the measurements. Samples were analyzed by applying a heating ramp from 0 °C to 120 °C, with an heating rate of 20 °C/min. Measurements were performed in duplicate. Data were analyzed with Trios v5.1.1.46572 software (TA Instruments).

2.3.9. Inductively coupled plasma-atomic emission spectrometry (ICP-OES)

The amount of released silver was determined using an Agilent 720-ES Inductively coupled plasma-atomic emission spectrometer (ICP-OES) equipped with a pneumatic nebulizer and a cyclonic spray chamber. The calibration lines were obtained by preparing the standard solutions starting from commercial standards certified at 1000 ppm. Silver absorbance was evaluated at 328.068 nm. After each measurement, the system was washed with a 2 % HNO_3 solution. Measurements were performed in triplicate, and the results are expressed as μg of Ag^+ released *per* mg of fiber.

2.3.10. Mechanical tests

A Discovery DHR-3 rheometer (TA Instruments) was used to evaluate the mechanical properties of the fibers. The latter were fixed to a paper support using bicomponent glue and clamped (Alves Fidelis et al., 2013; Tordi et al., 2023), applying a force equal to 30 cN·m (see Fig. S2 for details). The traction test was performed with a 10 μm/s rate. Measurements were performed in quadruplicate and the data were analyzed using Trios v5.1.1.46572 software (TA Instruments).

2.4. Ag release experiment

The release of Ag from the fibers upon incubation in water was performed by placing about 10 cm of each sample (dry fibers) in a glass vial filled with 10 mL of MilliQ water. The vials were kept at room temperature in an orbital shaker for 24 h. Afterwards, the incubating solutions were collected and analyzed to determine the amount of released Ag (see Section 2.3.9). The fibers were dried under the fume hood and imaged by means of FE-SEM to check for the presence of AgNPs. The experiment was carried out in triplicate.

2.5. Stability against dissolution

The stability against dissolution of the AgAlg sample was tested by immersing about 4 cm of dry fiber in 8 mL of MilliQ water. The samples were kept at room temperature in the orbital shaker and collected after 1, 3, 7, 10 and 14 days of incubation. The fibers were recovered from the solution and dried under the fume hood. When a constant weight was attained, their mass was recorded and compared with the mass before incubation, to obtain the weight % as a function of time. The test was performed in triplicate, and the average weight % ± SD was reported.

3. Results and discussion

3.1. In situ AgNPs synthesis

Phase separation, diffusion and rheological phenomena strongly influence the characteristics of polymeric fibers obtained through wet spinning (Rohani Shirvan et al., 2022). Mastering these aspects, especially in the crucial coagulation step, allowed us to obtain alginate fibers with a length of some meters with captivating properties despite the relatively weak interaction between alginate and Ag^+ ions (see Fig. 1b) (Qin, 2005, 2008). These fibers were treated with lemon juice to reduce Ag^+ to metallic silver by directly immersing the extruded and washed alginate fibers into a filtered solution of freshly-squeezed commercial lemons. The reduction was monitored for 30 min by observing the color of the fibers during the process (see Fig. 2a). In a few minutes, the fiber color changes from pale yellow to orange, then it goes brown (~ 10 min) and eventually black. This evolution reasonably indicates the successful formation of AgNPs within the alginate fiber, due to the reduction of the Ag^+ ions that crosslink the polymeric chain. The progressive color change suggests that the process occurs gradually. The dried fiber reduced for 30 min with the lemon juice was imaged by means of FE-SEM: the micrographs shown in Fig. 2b confirm the formation of AgNPs, both isolated and agglomerated into small clusters, on the fiber surface.

Aiming at understanding how the use of different CA/AA ratios in the reducing solution of the AgAlg fibers affects the Ag nanostructures formed on the fibers and their properties, we prepared a series of solutions with different content of CA and AA. The composition of the solutions, given in Table 1, was inspired by the average composition of lemon juice, which corresponds to sample AgAlg_CA/AA = 105 (Haytowitz et al., 2019). The color evolution of the AgAlg fibers reduced in the different solutions is displayed in Fig. 3a. AgAlg, which is shown as a reference, does not change its color during the experiment, confirming that the color variations observed in the other samples are solely due to the chemical reduction driven by AA and CA and not to uncontrolled photoreduction of Ag^+. The color evolution of the other samples dramatically depends on the reducing solution used. AgAlg_AA turns light brown in a few minutes, suggesting that AA alone at the same concentration found in lemon juice (see Table 1) is able to form Ag nanostructures on the fibers. AgAlg_CA/AA = 5, which is prepared in the reducing solution with the highest amount of AA, immediately turns black. Samples AgAlg_CA/AA = 25 and AgAlg_CA/AA = 50 also become black, but the color progression is more gradual, and a transition from yellow, to orange, to brown is observed. A progressive color evolution is also observed for AgAlg_CA/AA = 105 and AgAlg_CA/AA = 150 which, after 30 min of reduction, retain a brown and reddish color, respectively. Interestingly, AgAlg reduced in the solution containing only CA becomes pale yellow at the end of the process. This simple test suggests that with the increase of CA/AA ratio, the reduction is slower, and the different

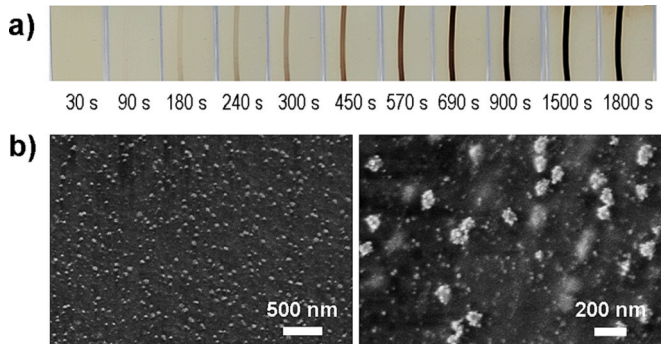

Fig. 2. a) Photos in time (from the left to the right) of the AgAlg fiber immersed in lemon juice. b) FE-SEM micrograph of the surface of AgAlg fibers reduced using lemon juice.

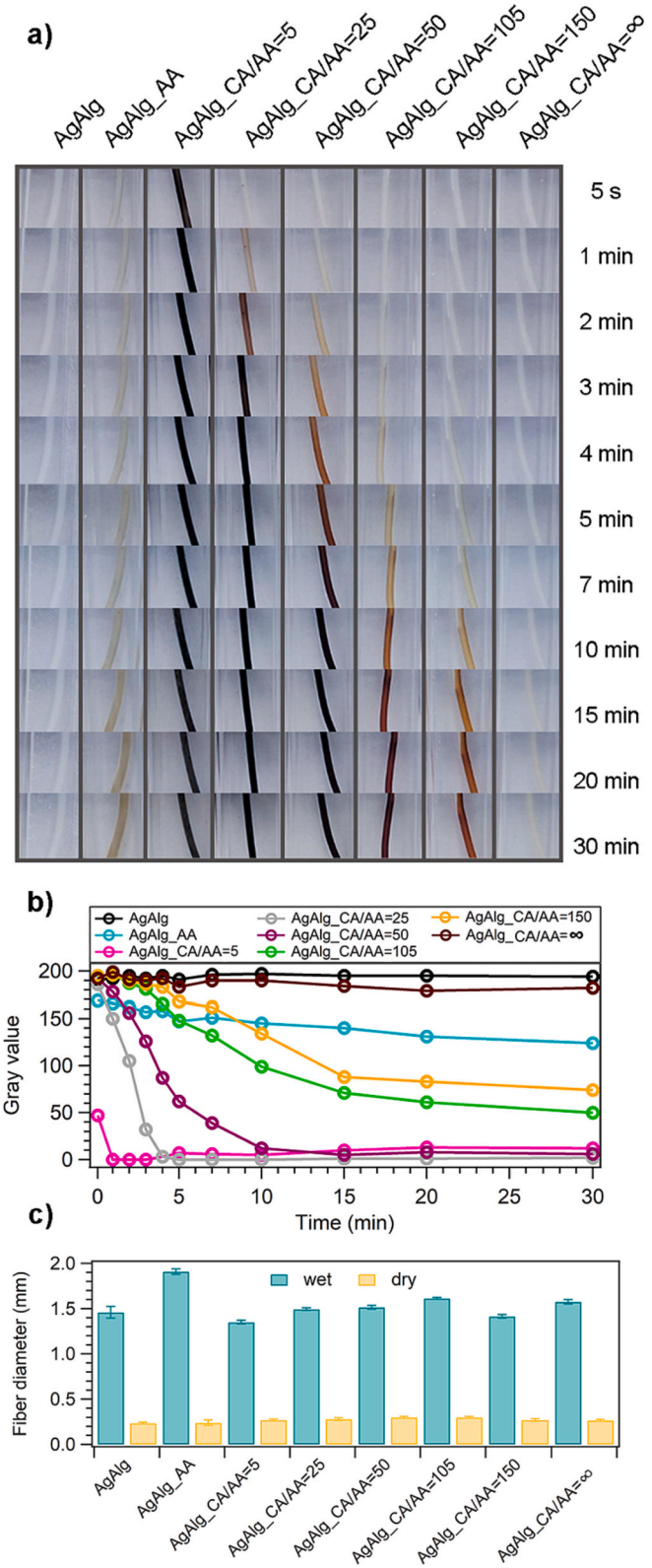

Fig. 3. a) Photos of the evolution in time of AgAlg fibers in the CA/AA solutions. b) Plot of the gray value sampled at half height of each specimen as a function of time (see Section 2.3.1). c) Diameter of the wet and dry fibers obtained from the optical microscopy images in Fig. S3. The error bar refers to the average ± SD of 10 measurements. The diameters of the wet fibers are the ones at the end of the preparation.

color obtained at the end of the reduction indicates a difference in the size/morphology/aggregation of the Ag nanostructures on the fibers. The color evolution in time could be quantified by converting the images in grayscale, and plotting the gray value in the middle of the fiber as a function of time (see the details in Section 2.3.1). The results reported in Fig. 3b corroborate the previous observations: the color of AgAlg is constant all over the experiment, showing a gray value compatible with a light gray color (about 200), slightly above AgAlg_CA/AA = ∞. AgAlg_CA/AA = 5 is also constant, but with a gray value close to 0 (black). All the other samples gradually decrease their gray value, in agreement with a slow color variation which depends on CA/AA ratio.

The diameter of the fibers at the end of the process was measured, and the results are given in Fig. 3c and Fig. S3. All samples except AgAlg_AA have a diameter around 1.5 mm, while that of AgAlg_AA is around 1.9 mm. Considering that the internal diameter of the needle used during the extrusion is 0.9 mm, a significant swelling of the fiber occurs during the crosslinking, reduction and washing steps. The measured maximum diameter of the wet AgAlg sample (*i.e.* 1.53 mm resulting from 1.46 mm ± 0.07 mm, see Fig. 3c), considerably higher than the one of the needle, is due to formation of the insoluble hydrogel structure that hampers the flow of the polymeric solution. Taking into account the amount of alginate solution extruded, the theoretical length of the extruded fiber is 2.62 m. The result is not far from the experimental value obtained (*i.e.* ~ 2.5 m): the mismatch can be attributed to the amount of polymer that diffuses into the Ag^+ solution during the crosslinking. Upon drying, the diameter of the fibers decreases up to about 0.3 mm, therefore a size reduction of about five times occurs.

3.2. Water absorption properties

The amount of water that the dried fibers are able to absorb when immersed in water was estimated with a swelling experiment, described in Section 2.3.3. The results reported in Fig. 4a show the swelling ratio (SR) as a function of time; in Eq. 1, the m_0 values (dried mass of the samples at the beginning of the experiment) were normalized for the different amount of water present in the dry fibers, estimated by means of TGA (see Fig. S4 and Table S3). The results show that different samples display a remarkably different swelling behavior. The non-reduced AgAlg fiber, when immersed in water, undergoes a negligible swelling (SR ~ 0.1). The fiber reduced only with AA has a modest SR at equilibrium (SR ~ 4). This phenomenon is due to the dishomogeneous distribution of reduced silver in that sample: regions with high silver content irreversibly collapse during dehydration and are not able to swell anymore. Interestingly enough, the fibers reduced in solution containing CA and AA are characterized by a SR at equilibrium between ~28 and ~ 47, its value being directly proportional to the CA/AA ratio in the range 5–105 (see Fig. 4b). This linear relationship makes it possible to obtain Ag-alginate fibers with predictable swelling ability in this CA/AA range. The reason for the different behavior of the samples in terms of swelling might be due to differences in the structure of the polymeric network induced by Ag^+ reduction: we can imagine that in AgAlg, all silver ions interact with the carboxylate groups of alginate, tightening the polymeric chains and hampering their interaction with water. When Ag^+ is reduced to metallic Ag, part of it is no longer able to crosslink alginate chains: as a consequence, the polymeric network is loosened and it is easier for water to penetrate the structure and swell it.

3.3. Morphological and elemental characterization

The morphology of the Ag nanostructures formed on the fibers was assessed with FE-SEM. The micrographs showing the outer surface of the samples are given in Fig. 5. While AgAlg displays the smooth surface typical of polymers, all other samples are covered by small inorganic structures with a size from tens to hundreds of nm, which reasonably consist of the AgNPs produced during the reduction. AgAlg_AA is covered by NPs with a size of tens of nm together with larger aggregated

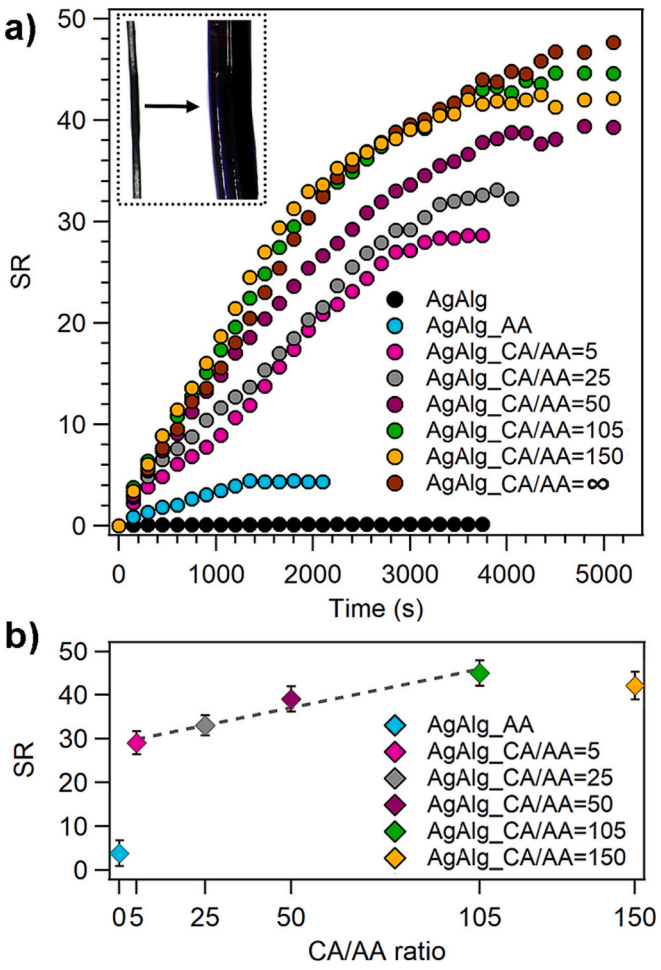

Fig. 4. a) Swelling curves of the samples. The inset shows the image of a fiber at the beginning (left) and at the end (right) of the experiment. Representative curves are reported for each sample. b) Plot of the SR at equilibrium as a function of the CA/AA ratio of the samples (SD was used as error bar). The equation of the line that interpolates the data between CA/AA = 5–105 is $y = 0.16x + 29.0$, r^2: 0.98.

clusters with an irregular shape. AgAlg_CA/AA = 5 (Fig. 5c) is characterized by irregular objects with a size of hundreds of nm: we can hypothesize that the very fast reduction of Ag^+ occurring in this sample (see the photos in Fig. 3a) leads to an uncontrolled formation of Ag nanostructures, in which the growth step is favored with respect to the nucleation. In the other samples, in which the reduction is more gradual given the higher CA/AA ratio, a higher amount of Ag nuclei forms, resulting in a decrease of the size of the object with decreasing AA amount in the reducing solution. Out of note, samples from CA/AA = 50 to CA/AA = 150 are characterized by AgNPs both spherical and cubic (the latter are more abundant in AgAlg_CA/AA = 50 sample, see Fig. 5e). It is also worth mentioning that despite AgAlg_AA and AgAlg_CA/AA = 105 were prepared with the same amount of AA in the reducing solution, the AgNPs morphology and distribution is markedly different (see Fig. 5b and f): the presence of CA might therefore contribute to the stabilization and dispersion of the small NPs on the alginate fiber, preventing the formation of large clusters. The observation of the fiber external surface also suggests that samples with a low CA/AA have the polymeric surface completely covered by Ag nanostructures, whereas in samples reduced in solutions with a low amount of AA the smaller NPs are not able to entirely cover the polymeric surface of the sample. This evidence might be related to the different swelling behavior of the samples previously discussed: the progressive increase in the SR with the increase of CA/AA (see Fig. 4) might indicate an easier access for water

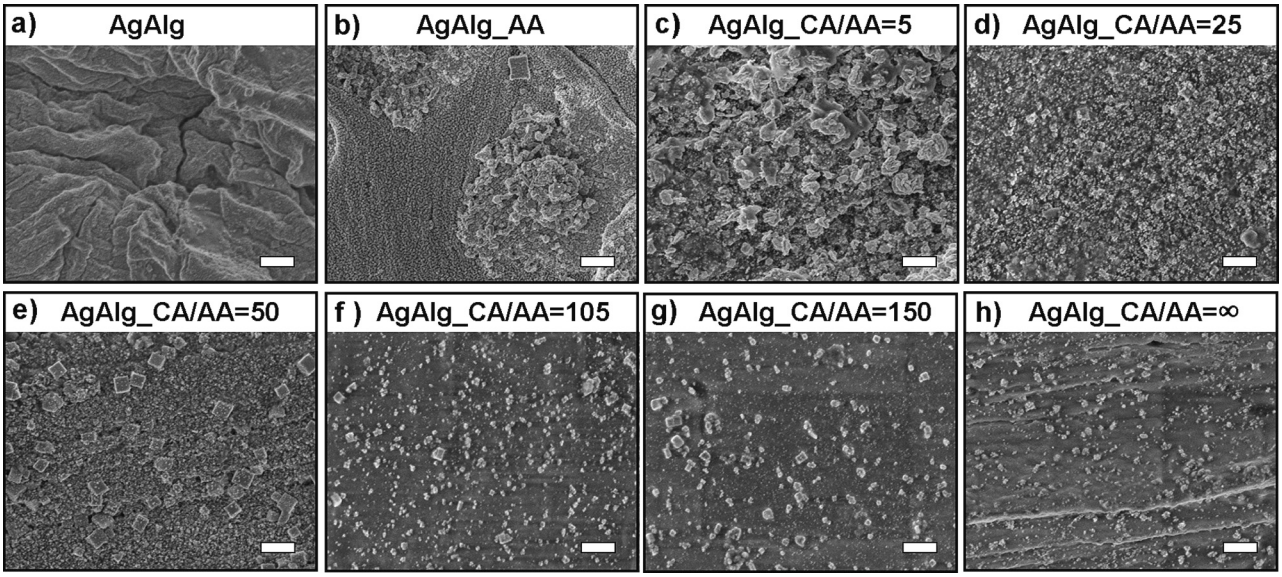

Fig. 5. FE-SEM micrographs of the surface of the dried fibers. The scale bar is 500 nm.

molecules to the hydrophilic polymeric chains in samples with low AA amount, thus resulting in a high swelling ability. In contrast, for samples with low CA/AA the fiber surface is entirely covered by metallic Ag, which hampers water interaction with the polymeric chains resulting in a lower swelling ability.

To understand if the specific morphology of the samples was induced by the drying process, we also imaged samples which were freeze-dried immediately after the last washing step of the preparation. The FE-SEM micrographs, reported in Fig. S5, reveal that all the samples have a morphology similar to the dried one. With the freeze-dried samples it was also possible to image the internal portion of the fibers, which is shown in Fig. S6. All samples are characterized by a porous network, with pore size of hundreds of nm. Qualitatively, the size of the pores appears to increase with the decrease in AA amount in the reducing solution. In order to understand if the formation of AgNPs also occurs within the fibers or if it is restricted to their surface, the cross-sections of each sample were imaged with SEM, and the results are shown in Fig. S7. For sample AgAlg_AA and AgAlg_CA/AA = 5 it was possible to detect Ag nanostructures also in the inner portion of the fiber, whereas for all the other samples no nanoparticles could be observed in the internal regions, suggesting that AgNPs formation mainly occurs on the fibers' surface.

The elemental composition of the fiber samples was investigated by coupling EDX analysis with SEM imaging. The results obtained from the EDX analysis of the samples in Fig. 5 are reported in Table S4 and confirm the presence of Ag in all the prepared fibers, together with C and O constituting the polymeric network. Out of note, the amount of Ag % decreases with the increase in CA/AA, in agreement with the amount of Ag nanostructures observed in SEM micrographs (see Fig. 5). <1 % of Na and Cl is found in all samples (Na likely comes from the residual ions of the sodium alginate that were not washed away or replaced by Ag^+ during the crosslinking). This very small amount of NaCl could also be responsible for a small portion of the cubic structures observed in the SEM images, as both Ag and NaCl are known to crystallize into cubic lattice structures. It has to be though remarked that considering the relative abundance of the two materials, NaCl cannot account for all the cubic structures observed on the fibers surfaces, which are therefore largely due to AgNPs.

Considering that Ag is present in our samples both as the crosslinking cation and as the constituent of the Ag nanostructures observed on the fibers (except for AgAlg sample), we aimed at further characterizing their crystallinity through XRD analysis. The patterns are reported in Fig. S8 and confirm that all the reduced samples but AgAlg_CA/AA = ∞ show the distinctive peaks of AgNPs (Fatemeh et al., 2017). On a qualitative basis, we can observe that the peak related to the (111) reflection (2θ = 38°) broadens as the CA/AA increases, in agreement with the average smaller size of the AgNPs pointed out in SEM micrographs (see Fig. 5). The pattern of AgAlg_CA/AA = ∞ does not show the peaks typical of Ag, likely due to the low amount evidenced by EDX. Interestingly, this sample shows two low intensity peaks at 2θ = 32.3° and 46.3°, which are compatible with both Ag_2O (Fowsiya & Madhumitha, 2019) and NaCl (Qin et al., 2017).

3.4. Alginate-Ag^+ interaction through FT-IR spectroscopy

The FT-IR spectra of all the prepared fibers are reported in Fig. 6 together with those of Sodium alginate and Alginic acid samples as references.

The full assignment of the spectra, based on literature data (Filipiuk et al., 2005; Papageorgiou et al., 2010), is reported in Table S7, while the assignment of the bands related to the -COO vibrations is reported in Table 2. The analysis of the FT-IR spectra of both AA (Yohannan Panicker et al., 2006) and CA (Bichara et al., 2011) (Fig. S9, Tables S5 and S6 in the Supplementary Material) testifies that the washing procedure completely removes these substances from the polymeric matrix of the fibers. The region between 1750 cm^{-1} and 1350 cm^{-1} provides useful information on the influence of both the crosslinking and the reducing treatment on the properties of the starting polymer backbone. The coordination of Ag^+ by the carboxylate groups shifts the absorption band related to the *asym*metric stretching of $-COO^-$ groups [$\nu(COO^-_{asym})$] to lower energies. The coordination does not alter the symmetric $-COO^-$ stretching band [$\nu(COO^-_{sym})$] and no other peaks appear/shift in this area. Treating AgAlg with AA alone partially protonates the carboxylate groups as testified by the absorption band at 1726 cm^{-1} in the spectrum of AgAlg_AA. This band is present in the Alginic acid spectrum and becomes more intense when also CA is used for the Ag^+- reduction (*i.e.*, AgAlg_CA/AA = X samples), reasonably due to the lower pH of the reducing formulations (see Section 2.2.2). The work of Nakamoto allows one to determine the geometry of metal-carboxylate complexes simply by evaluating the difference in energy between the $-COO^-$ stretching bands (both the symmetric and the asymmetric) (Nakamoto, 1986). Metal-carboxylate complexes can assume the three different geometries reported in Fig. 6: monodentate, bidentate chelating and bidentate bridging. By using Eq. (2), the values of $\Delta\nu_{Ag}$ and $\Delta\nu_{Na}$ were determined

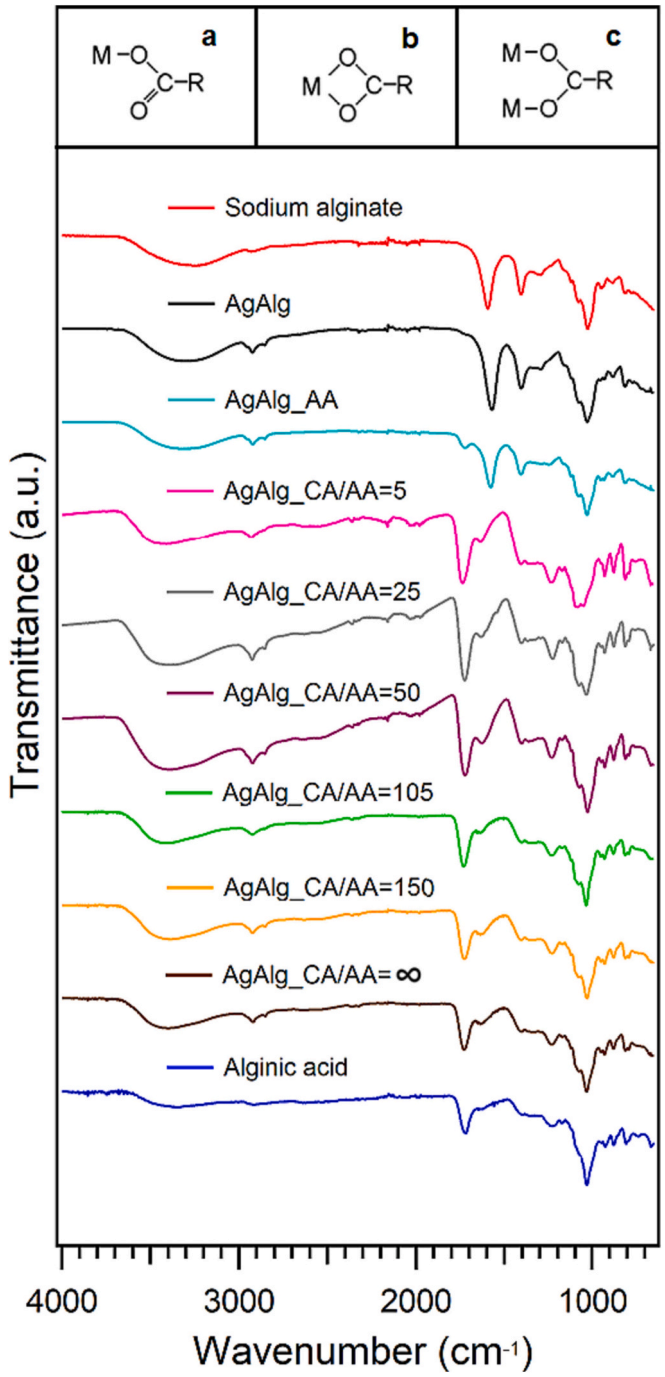

Fig. 6. FT-IR spectra of Sodium alginate (red), AgAlg (black), AgAlg_AA (light blue), AgAlg_CA/AA = 5 (pink), AgAlg_CA/AA = 25 (gray), AgAlg_CA/AA = 50 (purple), AgAlg_CA/AA = 105 (green), AgAlg_CA/AA = 150 (yellow), AgAlg_CA/AA = ∞ (brown) and Alginic acid (blue). The spectra were offset along the y axis for display purposes. In the a, b and c panels on top, the different coordination geometries of the metal-carboxylate complexes: monodentate (a), bidentate chelating (b) and bidentate bridging (c). All the spectra were normalized to the *ν(CO) + δ(CCO) + δ(CC)* band, except for AgAlg_CA/AA = 5 that was normalized to the *ν(OCO) ring* band (see Table S7). (For interpretation of the references to color in this figure legend, the reader is referred to the web version of this article.)

and compared. $\Delta\nu_{Ag}$ values higher, equal or lower than $\Delta\nu_{Na}$ can be attributed to monodentate, bidentate bridging or bidentate chelating coordination modes, respectively (Nakamoto, 1986).

$$\Delta\nu = \nu_{COOasym} - \nu_{COOsym} \quad (2)$$

Table 2
Assignment of the FT-IR spectra reported in Fig. 6, in the 1750–1350 cm^{-1} region (Error: ± 2 cm^{-1}, instrumental resolution). The complete assignment of the spectra is reported in Table S7.

Sample	ν(COOH)	$\nu(COO)_{asym}$	$\nu(COO)_{sym}$
Sodium alginate	/	1594	1405
AgAlg	/	1571	1405
AgAlg_AA	1726	1579	1407
AgAlg_CA/AA = 5	1737	1633	1407
AgAlg_CA/AA = 25	1725	1635	1403
AgAlg_CA/AA = 50	1722	1629	1403
AgAlg_CA/AA = 105	1730	1635	1405
AgAlg_CA/AA = 150	1726	1635	1405
AgAlg_CA/AA = ∞	1728	1635	1405
Alginic acid	1718	1635	1397

In this case, since $\Delta\nu_{Na}$ - $\Delta\nu_{Ag}$ = (23 ± 4) cm^{-1}, it is possible to assess that alginate coordination of Ag^+ is bidentate chelating. This information is coherent with the inter- and intramolecular coordination geometries proposed by Hassan (Hassan, 1991). In the first case alginate can interact with either two carboxylate groups or one carboxylate and one hydroxyl group of two different alginate chains, forming a planar complex perpendicular to the plain of the polymeric chains. In the second case, silver coordinates the carboxylate groups of two adjacent glycosidic units (Hassan, 1991). Both options imply that a high quantity of silver can be loaded in the alginate matrix in the AgAlg sample. Analogous considerations cannot be drawn for the samples containing reduced silver, in which the shift of the *asym*metric -COO^- stretching band to higher energies is probably due to the protonation (see Alginic acid spectrum assignment in Table 2). For the determination of the binding character (in terms of Fraction of Ionic Bonding, FIB) in the Ag-alginate complex of the AgAlg samples, we used Eq. (3), proposed by Chen (Chen et al., 2002):

$$FIB = \frac{\nu(COOH) - \nu(COOAg)}{\nu(COOH) - \nu(COONa)} \quad (3)$$

where *ν(COOH)* is the IR absorption frequency of Alginic acid -COOH stretching (classic covalent bond), while ν(COOAg) and ν(COONa) are the asymmetric -COO^- stretching frequencies of the Ag^+-crosslinked samples and Sodium alginate (classic ionic bond), respectively. The obtained FIB value for AgAlg (1.19 ± 0.04) exceeds unity, as a consequence of the lower frequency of the asymmetric stretching in the -COOAg complex with respect to the -COONa one. This phenomenon is attributable to electronic delocalization on the carboxylate groups, due to polarization and electronic retro-donation phenomena that stabilize the complex (Chen et al., 2002). Except for the AgAlg_AA sample (FIB = 1.12 ± 0.04), which is the less protonated sample, all the other reduced AgAlg fibers are characterized by FIB values close to zero, as a consequence of the shift to higher energy experienced by the $\nu(COO^-_{asym})$.

3.5. Thermal properties

The TGA analysis allowed us to rationalize the evidence from the previously discussed techniques, providing precious quantitative insights relatable to both elemental composition and molecular structurization. The TGA curves of the prepared fibers are reported in Fig. 7a, together with the ones of Sodium alginate and Alginic acid reference samples. As clearly shown in Fig. 7a, the weight losses of the samples were compared in 4 significant regions (denoted as Region I, II, III, and IV in Table 3). The equilibration of the samples at the same humidity level (*i.e.,* RH 95 %) allows one to exclude that variations in the degradative profiles might be due to different environmental factors.

The evaluation of the TGA curves up to 130 °C provides information on the water amount taken up by the samples due to humidity. The introduction of Ag^+ ions in the alginate matrix clearly hampers its ability to absorb water from the environment: in fact Sodium alginate

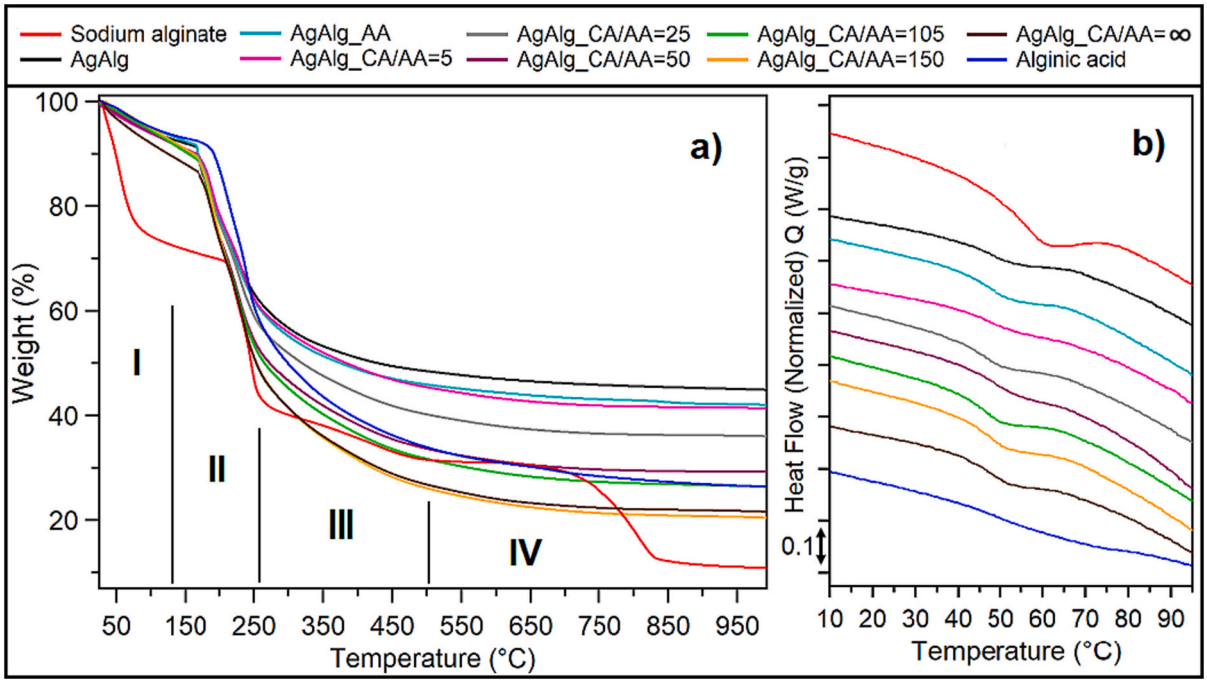

Fig. 7. TGA (a) and DSC (b) thermograms of Sodium alginate (red), AgAlg (black), AgAlg_AA (light blue), AgAlg_CA/AA = 5 (pink), AgAlg_CA/AA = 25 (gray), AgAlg_CA/AA = 50 (purple), AgAlg_CA/AA = 105 (green), AgAlg_CA/AA = 150 (yellow), AgAlg_CA/AA = ∞ (brown) and Alginic acid (blue). TGA thermograms (a): I (RT - 130 °C), II (130 °C - 260 °C), III (RT 260 °C - 505 °C), IV (505 °C - 1000 °C). DSC thermograms are offset for clearness. * TGA samples were equilibrated at RH 95 %, while the DSC ones were dried overnight in a ventilated environment (RH ~ 39 %, room temperature). (For interpretation of the references to color in this figure legend, the reader is referred to the web version of this article.)

contains about 20 % more water than AgAlg. The reducing treatment does not seem to have a strong impact on the water absorption properties of the Ag^+-crosslinked samples. This phenomenon can be attributed to the protonation of the polymer chains (highlighted with FT-IR spectroscopy): the acidic reducing agents protonate the carboxylate groups progressively released by Ag^+ during the formation of the AgNPs, making the samples more similar to Alginic acid, which shows a reduced tendency to interact with environmental humidity with respect to Sodium alginate. Another reason for the poor water vapor absorption properties of the AgNPs-containing samples is the huge amount of silver nanoparticles on the surface (see SEM section) that can act as a barrier towards the uptake of humidity. Probably the two hypotheses co-exist, as suggested by the analysis of the AgAlg_CA/AA = ∞ TGA curve. The latter contains the highest amount of water among all the reduced samples, probably due to the lack of a compact AgNPs coverage (no AA in the reducing formulation, see Table 1) and to the simultaneous protonation of the polymeric network. It is important to clarify that the first degradative event of the polymeric chains occurs in Region II (130 °C - 260 °C) (Ross et al., 2011). The onset of this phenomenon significantly varies as a function of the sample, as clearly shown in Table 3. The introduction of Ag^+ in the polymeric network strongly reduces thermal stability: the temperature onset of the first degradation event in the AgAlg sample is approximately 45 °C lower than Sodium alginate. This evidence suggests that replacing of Na^+ with the larger Ag^+ in the polymeric network increases the distance between the polymer chains, making them more susceptible to decarboxylation. Furthermore, the study of the conductivity of silver-alginate gels suggests that the coordination of silver can decarboxylate alginate in order to reduce Ag^+ ions, resulting in the production of free radicals (Hassan, 1991). The reduction with the sole AA does not influence the onset, while CA and mixtures of CA and AA produce samples with relatively higher thermal stability than that of AgAlg and AgAlg_AA samples. A homogeneous AgNPs distribution in a polymeric backbone is reportedly capable of stabilizing composites towards thermal degradation (Dash et al., 2021; Vodnik et al., 2009). Qualitatively, the degradation onset of the highly protonated fibers is smoother and resembles the one of the Alginic acid curve. In Table 3 the characteristic weight losses in specific temperature intervals are reported for each analyzed sample. Above 130 °C, it is useful to evaluate the weight losses normalized for the water content of the samples (Table 3). The weight loss in the 130 °C – 260 °C range is associated with the loss of the carboxylate groups in the form of CO and CO_2 from the polymer backbone (Ross et al., 2011). Fibers experience increasing weight losses (%) as the amount of AA used for the reduction decreases. This trend in the weight losses results in decreasing residues at the end of the thermal ramp (1000 °C, see Table 4) and can be attributed to the progressively reduced amount of silver in the samples highlighted performing TGA measurements in air on the same samples (see Fig. S10 and Table S8). Due to the absence of residue in the Alginic acid sample, it is possible to state that the residue at the end of the heating ramp is only due to the silver present in the samples. AgAlg is, as expected, the sample with the highest silver content (36.2 *w*/w % of the dried sample, Table 4). This result is particularly relevant since it indicates that the fiber obtained through the wet spinning approach contains 1 Ag^+ ion per monomeric unit of the alginate backbone, suggesting that only the bidentate chelating interaction between Ag^+ and carboxylate groups (elucidated by FT-IR Spectroscopy) is strong enough to maintain the inorganic species in the hydrogel through the washing cycles. This aspect is particularly interesting since it enables us to predict the amount of Ag^+ ions that can be loaded in the fibers as a function of the monomeric units present. It is interesting to note that an increasing amount of AA in the reducing formulation leads to an increase in the amount of silver in the fibers. The metal content is negligible in the case of AgAlg_CA/AA = 105, AgAlg_CA/AA = 150 and AgAlg_CA/AA = ∞ samples: this evidence suggests that a faster reduction implies a more efficient trapping of silver (in the form of AgNPs) in the polymeric network. AgAlg_AA is not coherent with the highlighted trend: this is probably due to the huge amount of silver quickly formed on the surface, which can easily be lost during the washing steps. The results also confirm that the protonation (highlighted through FT-IR Spectroscopy and forming the water insoluble alginic acid) is useful to preserve the

Table 3
TGA weight losses for the samples illustrated in Fig. 7a. Region I (RT - 130 °C), Region II (130 °C - 260 °C), Region III (RT 260 °C - 505 °C), Region IV (505 °C - 1000 °C). Data normalized for the water content of the samples are also reported (Norm. weight loss (%)). The error on the *Weight loss* associated with each sample never exceeds 1.0 %.

Sample	Region	Weight loss (%)	Norm. weight loss (%)	Onset I polymeric degradation
	I	27.5	0	
Sodium alginate	II	29.2	40.3	212.1 °C
	III	11.9	16.4	
	IV	20.5	28.3	
	I	7.2	0	
AgAlg	II	31.3	33.7	166.4 °C
	III	13.1	14.1	
	IV	3.5	3.7	
	I	6.6	0	
AgAlg_AA	II	33.3	35.7	166.0 °C
	III	14.3	15.3	
	IV	3.8	4.1	
	I	7.9	0	
AgAlg_CA/AA = 5	II	31.7	34.4	170.4 °C
	III	15.1	16.4	
	IV	3.9	4.2	
	I	7.9	0	
AgAlg_CA/AA = 25	II	35.3	38.3	169.5 °C
	III	16.8	18.2	
	IV	4.0	4.3	
	I	8.1	0	
AgAlg_CA/AA = 50	II	39.8	43.3	169.3 °C
	III	18.6	20.2	
	IV	4.3	4.7	
	I	8.1	0	
AgAlg_CA/AA = 105	II	40.9	44.5	171.8 °C
	III	19.5	21.2	
	IV	5.2	5.7	
	I	7.6	0	
AgAlg_CA/AA = 150	II	44.2	47.8	169.0 °C
	III	22.3	24.1	
	IV	5.4	5.8	
	I	10.5	0	
AgAlg_CA/AA = ∞	II	41.4	46.3	168.7 °C
	III	21.5	24.0	
	IV	5.0	5.6	
	I	6.4	0	
Alginic acid	II	36.2	38.7	187.5 °C
	III	23.7	25.3	
	IV	7.3	7.8	

filiform structure when Ag^+ abandons the coordination sites. The weight losses in the 260 °C - 1000 °C range (*i.e.* Region III and IV in Table 3, mainly connected to the degradation of the polymeric component) are similar for all the samples, except for Sodium alginate. In this case heating the sample produces Na_2CO_3 that decomposes to NaO and CO_2 around 700 °C (Soares et al., 2004).

The DSC thermograms of the analyzed samples are illustrated in Fig. 7b, while the evaluated glass transition temperatures (Tg) are reported in Table 4. All the samples were dried overnight in a ventilated environment (RH ~ 39 %, room temperature). The analysis on the AgAlg sample highlighted that the crosslinking process induces a shift (from 53.6 °C to 47.6 °C) of the Tg to lower temperatures. The higher dimension of Ag^+ with respect to Na^+ likely reduces the organization of the polymer chains, increasing their mobility. The different reducing treatments do not influence the glass transition temperature which remains comparable to the AgAlg sample, although the Alginic acid reference sample shows a Tg at higher temperature (50.2 °C). This phenomenon, considering the amount of silver in the samples, suggests that only the Ag^+-mediated crosslinking step alters the polymer chains mobility.

Table 4
Silver content (TGA under air flux, Fig. S10 and Table S8), degradative highlights (TGA under nitrogen flux, Fig. 7a and Table 3) and DSC (Fig. 7b) evaluation for the investigated samples. The error associated with each TGA value reported never exceeds 1.0 %.

Sample	Ag (w/w %)	Norm. Residue at 1000 °C (TGA)	Tg (DSC)
Sodium alginate	/	15.0 %	(53.6 ± 0.5) °C
AgAlg	36.2	48.5 %	(47.6 ± 0.8) °C
AgAlg_AA	24.7	44.9 %	(46.2 ± 0.5) °C
AgAlg_CA/AA = 5	27.3	45.0 %	(47.2 ± 0.4) °C
AgAlg_CA/AA = 25	21.3	39.2 %	(46.8 ± 0.4) °C
AgAlg_CA/AA = 50	13.3	31.8 %	(47.4 ± 0.5) °C
AgAlg_CA/AA = 105	~ 0	28.6 %	(46.3 ± 1.0) °C
AgAlg_CA/AA = 150	~ 0	22.3 %	(47.6 ± 0.6) °C
AgAlg_CA/AA = ∞	~ 0	24.1 %	(47.2 ± 0.4) °C
Alginic acid	/	26.4 %	(50.2 ± 0.6) °C

3.6. Silver release and mechanical properties evaluation

In the view of a possible application of the fibers in water purification systems, silver release experiments were performed (see Section 2.4 for details). The results of the ICP-OES analysis reported in Table 5 highlighted that AgAlg is the sample with the highest silver release over 24 h (*i.e.* ~ 9 μg of Ag^+ / mg of fiber). The reduction strongly reduces the amount of silver released in water by the samples (especially when both CA and AA are used), suggesting that this property can be tailored as a function of the preparation. It is interesting to note that, irrespectively of the total amount of silver in the samples (see Table 4), samples from CA/AA = 25 to CA/AA = ∞ show similar values of released Ag^+: this evidence suggests that the release of cations is mostly attributable to the silver-based structures present on the surface. The latter are still present on the surface after 24 h in water, as illustrated from the FE-SEM micrographs in Fig. S11. It is worth mentioning that the effectiveness of Ag^+ against bacteria was already proved for low silver concentrations (~ 0.08 mg/mL (Nawaz et al., 2012)), while the upper limit for the silver

Table 5
Silver release and mechanical properties (see Fig. S14) of the fibers. The release experiment was carried out in triplicate (mean ± SD), whereas the mechanical properties results are the average ± SD resulting from four replicated experiments. The Young's modulus (GPa) was evaluated for strain values between 0 and 0.01 for all the samples.

Sample	Ag^+ rel. / mg of fiber (μg)	Young's modulus (GPa)	Ultimate tensile strength (MPa)
AgAlg	9.05 ± 0.28	5.60 ± 0.36	108.9 ± 0.6
AgAlg_AA	1.47 ± 0.02	3.57 ± 0.47	61.2 ± 3.4
AgAlg_CA/AA = 5	0.39 ± 0.01	3.77 ± 0.19	86.5 ± 3.6
AgAlg_CA/AA = 25	0.82 ± 0.01	3.36 ± 0.51	82.4 ± 2.5
AgAlg_CA/AA = 50	0.73 ± 0.01	2.96 ± 0.05	68.5 ± 2.0
AgAlg_CA/AA = 105	0.77 ± 0.01	3.01 ± 0.33	64.4 ± 3.5
AgAlg_CA/AA = 150	0.71 ± 0.01	2.17 ± 0.38	72.1 ± 3.4
AgAlg_CA/AA = ∞	0.61 ± 0.01	3.42 ± 0.24	80.1 ± 1.1

content in drinking water set by US-EPA is equal to 0.1 mg/mL): the ability to control the release of silver from the composite matrix is crucial to satisfy law requirements without losing functionality. It is also important to remark that at the end of the release experiment all the fibers preserved their integrity (see Fig. S12). To further inspect the stability against dissolution of the AgAlg sample, we carried out an experiment to monitor its weight loss as a function of the incubation time. This test, which is useful in view of an application of AgAlg fibers in which the materials should be maintained in contact with aqueous media, can also give insights into the stability of the Ag^+-alginate complex. As described in Section 2.5, the weight change of the fiber was monitored in time up to 14 days (see Fig. S13), demonstrating an excellent stability against dissolution of the material (weight loss after 14 days: ~1 %).

Traction tests were also performed to characterize the mechanical properties of the fibers and the collected stress *vs* strain curves are reported in Fig. S14. AgAlg possesses the highest Young's modulus (*i.e.* ~ 5.60 GPa) and Ultimate tensile strength (*i.e.* ~ 108.9 MPa) among the analyzed samples (see Table 5), suggesting that the reduction increases the rigidity of the fibers, making them more brittle. All the reduced fibers are similar in terms of both Young's modulus and Ultimate tensile strength (see Table 5). It is interesting to note that AgAlg_AA is characterized by the shortest plastic deformation region that extends up to a maximum strain value of about 0.04. The protonation of the network experienced by the other reduced samples (highlighted through FT-IR spectroscopy, see Section 3.4), might be beneficial to maintain a certain plasticity after the Ag^+ removal from the silver-carboxylate complex.

4. Conclusions

In this work we demonstrated that the interaction between alginate and Ag^+ cations can be profitably exploited for the production of complex-shaped hydrogel structures such as fibers. The Ag^+-alginate interaction is commonly neglected by the scientific community, due to the poor bibliography regarding this topic and to the large variety of multivalent cations that can be chosen for the preparation of multi shaped hydrogels. Nevertheless, silver possesses unique antimicrobial properties that make it particularly attractive. The wet spinning approach for the preparation of Ag^+-crosslinked alginate fibers here reported, although simple and capable of maximizing the quantity of loaded silver, is unprecedented in the literature due to the "weak" interaction between Ag^+ and alginate that strongly reduces the chances of success. However, we proved that the optimization of a few experimental parameters enabled us to reach our goal.

We took advantage of the "weak" Ag^+-alginate interaction to decorate the polymeric fibers with AgNPs, which were obtained from the reduction of Ag^+ ions with a mild reducing agent, *i.e.* lemon juice-mimicking AA and CA solutions. We demonstrated that both the aforementioned molecules act as reducing agents and that peculiar properties can be imparted to the fibers varying the CA/AA ratio. Specifically, SEM analysis highlighted that increasing amounts of AA lead to an increase in the silver nanostructure density on the fibers surface. The observation of the color variation during the process also highlighted that higher amounts of AA lead to a faster reduction of the Ag^+ ions. FT-IR spectroscopy allowed us to determine a bidentate chelating coordination mode for the carboxylate group in the Ag^+-crosslinked fibers and to follow the impact of preparation steps on the polymeric structure. The use of CA clearly promotes the protonation of the polymer chains, strongly influencing the properties of the fibers. Thermogravimetric analysis highlighted that the introduction of silver in the network reduces the thermal stability, while the reduction leads to a slight increase of the latter. Furthermore this characterization unraveled the amount of silver contained in each sample, proving that it can be easily varied as a function of the amount of AA used. Also water absorption properties proved to be tunable as a function of the CA/AA ratio: the obtained swelling curves for AgNPs-containing samples indicate that the obtained fibers can be classified as super absorbents. It is worth mentioning that our preparation minimizes the number of steps required for the obtainment of the composite material. The latter is one of the many *Principles of Green Chemistry* respected by our preparation. Among them the use of reagents from renewable sources (alginate from algae, AA and CA from fruit) and the low energy consumption (only the extrusion step requires electricity) are undoubtedly fulfilled. These aspects, added to the biocompatibility and biodegradability of the used materials, suggest a promising future of such fibers in many fields, such as wound healing or in water/air purification processes.

CRediT authorship contribution statement

Pietro Tordi: Investigation, Formal analysis, Writing – original draft. **Rita Gelli:** Investigation, Formal analysis, Writing – original draft. **Francesca Ridi:** Conceptualization, Supervision, Writing – review & editing. **Massimo Bonini:** Conceptualization, Supervision, Writing – review & editing, Project administration.

Declaration of competing interest

The authors declare that they have no known competing financial interests or personal relationships that could have appeared to influence the work reported in this paper.

Data availability

Data will be made available on request.

Acknowledgments

CSGI (Consorzio Interuniversitario per lo Sviluppo dei Sistemi a Grande Interfase) and MUR-Italy ("Progetto Dipartimenti di Eccellenza 2023−2027" allocated to Department of Chemistry "Ugo Schiff") are acknowledged for the financial support. Prof. Mirko Severi is acknowledged for the ICP-OES measurements.

Appendix A. Supplementary data

Supplementary data to this article can be found online at https://doi.org/10.1016/j.carbpol.2023.121586.

References

Aarstad, O., Strand, B. L., Klepp-Andersen, L. M., & Skjåk-Bræk, G. (2013). Analysis of G-block distributions and their impact on gel properties of in vitro epimerized mannuronan. *Biomacromolecules, 14*(10), 3409–3416. https://doi.org/10.1021/bm400658k

Alves Fidelis, M. E., Pereira, T. V. C., Gomes, O. D. F. M., De Andrade Silva, F., & Toledo Filho, R. D. (2013). The effect of fiber morphology on the tensile strength of natural fibers. *Journal of Materials Research and Technology, 2*(2), 149–157. https://doi.org/10.1016/j.jmrt.2013.02.003

Ambrogi, V., Pietrella, D., Donnadio, A., Latterini, L., Di Michele, A., Luffarelli, I., & Ricci, M. (2020). Biocompatible alginate silica supported silver nanoparticles composite films for wound dressing with antibiofilm activity. *Materials Science and Engineering: C, 112*, Article 110863. https://doi.org/10.1016/j.msec.2020.110863

Bichara, L. C., Lanús, H. E., Ferrer, E. G., Gramajo, M. B., & Brandán, S. A. (2011). Vibrational study and force field of the citric acid dimer based on the SQM methodology. *Advances in Physical Chemistry, 2011*, 1–10. https://doi.org/10.1155/2011/347072

Chen, J. P., Hong, L., Wu, S., & Wang, L. (2002). Elucidation of interactions between metal ions and ca alginate-based ion-exchange resin by spectroscopic analysis and modeling simulation. *Langmuir, 18*(24), 9413–9421. https://doi.org/10.1021/la026060v

Dash, K. K., Kumar, A., Kumari, S., & Malik, M. A. (2021). Silver nanoparticle incorporated flaxseed protein-alginate composite films: Effect on physicochemical, mechanical, and thermal properties. *Journal of Polymers and the Environment, 29*(11), 3649–3659. https://doi.org/10.1007/s10924-021-02137-y

Durán, N., Durán, M., de Jesus, M. B., Seabra, A. B., Fávaro, W. J., & Nakazato, G. (2016). Silver nanoparticles: A new view on mechanistic aspects on antimicrobial activity.

Nanomedicine: Nanotechnology, Biology and Medicine, 12(3), 789–799. https://doi.org/10.1016/j.nano.2015.11.016

Elhoudi, M., Oukhrib, R., A. Celaya, C., G. Araiza, D., Abdellaoui, Y., Barra, I., Brahmi, Y., Bourzi, H., Reina, M., Albourine, A., & Abou Oualid, H. (2022). Comparison of green bio-based cerium/alginate vs. copper/alginate beads: A study of vibrational and thermal properties using experimental and theoretical methods. *Journal of Molecular Modeling, 28*(2), 37. https://doi.org/10.1007/s00894-022-05028-8

El-Naggar, N. E.-A., Hussein, M. H., & El-Sawah, A. A. (2017). Bio-fabrication of silver nanoparticles by phycocyanin, characterization, in vitro anticancer activity against breast cancer cell line and in vivo cytotxicity. *Scientific Reports, 7*(1), 10844. https://doi.org/10.1038/s41598-017-11121-3

Fatemeh, K., Mohammad Javad, M., & Samaneh, K. (2017). The effect of silver nanoparticles on composite shear bond strength to dentin with different adhesion protocols. *Journal of Applied Oral Science, 25*, 367–373. https://doi.org/10.1590/1678-7757-2016-0391

Filipiuk, D., Fuks, L., & Majdan, M. (2005). Transition metal complexes with uronic acids. *Journal of Molecular Structure, 744–747*, 705–709. https://doi.org/10.1016/j.molstruc.2004.11.073

Fowsiya, J., & Madhumitha, G. (2019). Biomolecules derived from Carissa edulis for the microwave assisted synthesis of Ag2O nanoparticles: A study against S. Incertulas, C. Medinalis and S. mauritia. *Journal of Cluster Science, 30*(5), 1243–1252. https://doi.org/10.1007/s10876-019-01627-3

Gómez-Ordóñez, E., & Rupérez, P. (2011). FTIR-ATR spectroscopy as a tool for polysaccharide identification in edible brown and red seaweeds. *Food Hydrocolloids, 25*(6), 1514–1520. https://doi.org/10.1016/j.foodhyd.2011.02.009

Grasdalen, H. (1983). High-field, 1H-n.m.r. spectroscopy of alginate: Sequential structure and linkage conformations. *Carbohydrate Research, 118*, 255–260. https://doi.org/10.1016/0008-6215(83)88053-7

Grasdalen, H., Larsen, B., & Smidsrød, O. (1979). A p.m.r. study of the composition and sequence of uronate residues in alginates. *Carbohydrate Research, 68*(1), 23–31. https://doi.org/10.1016/S0008-6215(00)84051-3

Grasdalen, H., Larsen, B., & Smisrod, O. (1981). 13C-n.m.r. studies of monomeric composition and sequence in alginate. *Carbohydrate Research, 89*(2), 179–191. https://doi.org/10.1016/S0008-6215(00)85243-X

Hassan, R. (1991). Alginate polyelectrolyte ionotropic gels 7. Physicochemical studies on silver(I) alginate complex with special attention to the electrical conductance and geometrical structure. *Colloids and Surfaces, 60*, 203–212. https://doi.org/10.1016/0166-6622(91)80278-V

Haug, A., & Smidsrød, O. (1965). The effect of divalent metals on the properties of alginate solutions. II. Comparison of different metal ions. *Acta Chemica Scandinavica, 19*, 1947–1949.

Haug, H., Larsen, B., & Smidsrød, O. (1967). Studies of uronic acid residues in alginic acid. In , *21. Acta Chemica Scandinavica* (pp. 691–704).

Haytowitz, D. B., Ahuja, J. K. C., Wu, X., Somanchi, M., Nickle, M., Nguyen, Q. A., Roseland, J. M., Williams, J. R., Patterson, K. Y., Li, Y., & Pehrsson, P. R. (2019). USDA National Nutrient Database for standard reference, Legacy Release. Nutrient Data Laboratory, Beltsville Human Nutrition Research Center, ARS, USDA. https://data.nal.usda.gov/dataset/usda-national-nutrient-database-standard-reference-legacy-release.

Huang, H., & Larsen, B. (1962). Quantitative determination of the uronic acid composition of alginates. In , *16. Acta Chemica Scandinavica* (pp. 1908–1918).

Lengert, E., Saveleva, M., Abalymov, A., Atkin, V., Wuytens, P. C., Kamyshinsky, R., … Parakhonskiy, B. (2017). Silver alginate hydrogel micro- and nanocontainers for theranostics: Synthesis, encapsulation, remote release, and detection. *ACS Applied Materials & Interfaces, 9*(26), 21949–21958. https://doi.org/10.1021/acsami.7b08147

Lin, S., Huang, R., Cheng, Y., Liu, J., Lau, B. L. T., & Wiesner, M. R. (2013). Silver nanoparticle-alginate composite beads for point-of-use drinking water disinfection. *Water Research, 47*(12), 3959–3965. https://doi.org/10.1016/j.watres.2012.09.005

Mane Gavade, S. J., Nikam, G. H., Dhabbe, R. S., Sabale, S. R., Tamhankar, B. V., & Mulik, G. N. (2015). Green synthesis of silver nanoparticles by using carambola fruit extract and their antibacterial activity. *Advances in Natural Sciences: Nanoscience and Nanotechnology, 6*(4), Article 045015. https://doi.org/10.1088/2043-6262/6/4/045015

Masuelli, M., & Illanes, C. (2014). Review of the characterization of sodium alginate by intrinsic viscosity measurements. *Comparative analysis between conventional and single point methods, 1*, 1–11.

Nakamoto, K. (1986). Complexes of alcohols, ethers, ketones, aldehydes, esters, and carboxylic acids. In *Infrared and Raman spectra of inorganic and coordination compounds* (pp. 231–233). Wiley interscience.

Nawaz, M., Han, M. Y., Kim, T., Manzoor, U., & Amin, M. T. (2012). Silver disinfection of Pseudomonas aeruginosa and E. Coli in rooftop harvested rainwater for potable purposes. *The Science of the Total Environment, 431*, 20–25. https://doi.org/10.1016/j.scitotenv.2012.05.022

Ortega, F., Arce, V. B., & Garcia, M. A. (2021). Nanocomposite starch-based films containing silver nanoparticles synthesized with lemon juice as reducing and stabilizing agent. *Carbohydrate Polymers, 252*, Article 117208. https://doi.org/10.1016/j.carbpol.2020.117208

Papageorgiou, S. K., Kouvelos, E. P., Favvas, E. P., Sapalidis, A. A., Romanos, G. E., & Katsaros, F. K. (2010). Metal–carboxylate interactions in metal–alginate complexes studied with FTIR spectroscopy. *Carbohydrate Research, 345*(4), 469–473. https://doi.org/10.1016/j.carres.2009.12.010

Porter, G., Schwass, D., Tompkins, G., Bobbala, S., Medlicott, N., & Meledandri, C. (2021). AgNP/alginate nanocomposite hydrogel for antimicrobial and antibiofilm applications. *Carbohydrate Polymers, 251*. https://doi.org/10.1016/j.carbpol.2020.117017

Prathna, T. C., Chandrasekaran, N., Raichur, A. M., & Mukherjee, A. (2011). Biomimetic synthesis of silver nanoparticles by Citrus Limon (lemon) aqueous extract and theoretical prediction of particle size. *Colloids and Surfaces. B, Biointerfaces, 82*(1), 152–159. https://doi.org/10.1016/j.colsurfb.2010.08.036

Qin, Y. (2005). Silver-containing alginate fibres and dressings. *International Wound Journal, 2*(2), 172–176. https://doi.org/10.1111/j.1742-4801.2005.00101.x

Qin, Y. (2008). Alginate fibres: An overview of the production processes and applications in wound management. *Polymer International, 57*(2), 171–180. https://doi.org/10.1002/pi.2296

Qin, Y., Yu, D., & Zhou, J. (2017). DNA action on the growth and habit modification of NaCl crystals. *CrystEngComm, 19*(36), 5356–5360. https://doi.org/10.1039/C7CE01148B

Qing, Z., Wang, L., Liu, X., Song, Z., Qian, F., & Song, Y. (2022). Simply synthesized sodium alginate/zirconium hydrogel as adsorbent for phosphate adsorption from aqueous solution: Performance and mechanisms. *Chemosphere, 291*, Article 133103. https://doi.org/10.1016/j.chemosphere.2021.133103

Ravichandran, V., Vasanthi, S., Shalini, S., Shah, S. A. A., Tripathy, M., & Paliwal, N. (2019). Green synthesis, characterization, antibacterial, antioxidant and photocatalytic activity of Parkia speciosa leaves extract mediated silver nanoparticles. *Results in Physics, 15*, Article 102565. https://doi.org/10.1016/j.rinp.2019.102565

Rohani Shirvan, A., Nouri, A., & Sutti, A. (2022). A perspective on the wet spinning process and its advancements in biomedical sciences. *European Polymer Journal, 181*, Article 111681. https://doi.org/10.1016/j.eurpolymj.2022.111681

Ross, A. B., Hall, C., Anastasakis, K., Westwood, A., Jones, J. M., & Crewe, R. J. (2011). Influence of cation on the pyrolysis and oxidation of alginates. *Journal of Analytical and Applied Pyrolysis, 91*(2), 344–351. https://doi.org/10.1016/j.jaap.2011.03.012

Sakugawa, K., Ikeda, A., Takemura, A., & Ono, H. (2004). Simplified method for estimation of composition of alginates by FTIR. *Journal of Applied Polymer Science, 93*(3), 1372–1377. https://doi.org/10.1002/app.20589

Salomonsen, T., Jensen, H. M., Larsen, F. H., Steuernagel, S., & Engelsen, S. B. (2009). Direct quantification of M/G ratio from (13)C CP-MAS NMR spectra of alginate powders by multivariate curve resolution. *Carbohydrate Research, 344*(15), 2014–2022. https://doi.org/10.1016/j.carres.2009.06.025

Shannon, R. D. (1976). Revised effective ionic radii and systematic studies of interatomic distances in halides and chalcogenides. *Acta Crystallogr. Sect. A, 32*(5), 751–767. https://doi.org/10.1107/S0567739476001551

Singh, P., Singh, S. K., Bajpai, J., Bajpai, A. K., & Shrivastava, R. B. (2014). Iron crosslinked alginate as novel nanosorbents for removal of arsenic ions and bacteriological contamination from water. *Journal of Materials Research and Technology, 3*(3), 195–202. https://doi.org/10.1016/j.jmrt.2014.03.005

Sivasankar, P., Seedevi, P., Poongodi, S., Sivakumar, M., Murugan, T., Sivakumar, L., Sivakumar, K., & Balasubramanian, T. (2018). Characterization, antimicrobial and antioxidant property of exopolysaccharide mediated silver nanoparticles synthesized by Streptomyces violaceus MM72. *Carbohydrate Polymers, 181*, 752–759. https://doi.org/10.1016/j.carbpol.2017.11.082

Skjåk-Bræk, G., Grasdalen, H., & Larsen, B. (1986). Monomer sequence and acetylation pattern in some bacterial alginates. *Carbohydrate Research, 154*(1), 239–250. https://doi.org/10.1016/S0008-6215(00)90036-3

Soares, J. P., Santos, J. E., Chierice, G. O., & Cavalheiro, E. T. G. (2004). Thermal behavior of alginic acid and its sodium salt. *Eclética Química, 29*, 57–64. https://doi.org/10.1590/S0100-46702004000200009

Stanford, E. C. C. (1881). *Improvements in the manufacture of useful products from seaweeds (patent British patent 142.40)*.

Tordi, P., Ridi, F., & Bonini, M. (2023). A green and sustainable approach for the preparation of Cu-containing alginate fibers. *Colloids and Surfaces A: Physicochemical and Engineering Aspects, 677*, Article 132396. https://doi.org/10.1016/j.colsurfa.2023.132396

Vetrano, A., Gabriele, F., Germani, R., & Spreti, N. (2022). Characterization of lipase from Candida rugosa entrapped in alginate beads to enhance its thermal stability and recyclability. *New Journal of Chemistry, 46*(21), 10037–10047. https://doi.org/10.1039/D2NJ01160C

Vodnik, V. V., Vuković, J. V., & Nedeljković, J. M. (2009). Synthesis and characterization of silver—Poly(methylmethacrylate) nanocomposites. *Colloid and Polymer Science, 287*(7), 847–851. https://doi.org/10.1007/s00396-009-2039-7

Yohannan Panicker, C., Tresa Varghese, H., & Philip, D. (2006). FT-IR, FT-Raman and SERS spectra of vitamin C. *Spectrochimica Acta Part A: Molecular and Biomolecular Spectroscopy, 65*(3), 802–804. https://doi.org/10.1016/j.saa.2005.12.044

Yoon, H. S., Andersen, R. A., Boo, S. M., & Bhattacharya, D. (2009). Stramenopiles. In M. Schaechter (Ed.), *Encyclopedia of microbiology* (3rd ed., pp. 721–731). Academic Press. https://doi.org/10.1016/B978-012373944-5.00253-4.

Zhou, Q., Lin, X., Li, B., & Luo, X. (2014). Fluoride adsorption from aqueous solution by aluminum alginate particles prepared via electrostatic spinning device. *Chemical Engineering Journal, 256*, 306–315. https://doi.org/10.1016/j.cej.2014.06.101